Building and Environment 104 (2016) 152–161

Contents lists available at ScienceDirect

Building and Environment

journal homepage: www.elsevier.com/locate/buildenv

Pore-scale modelling of dynamic interaction between SVOCs and airborne particles with lattice Boltzmann method

Yu-Tong Mu, Li Chen, Ya-Ling He, Wen-Quan Tao*

Key Laboratory of Thermo-Fluid Science & Engineering of MOE, School of Energy and Power Engineering, Xi'an Jiaotong University, Xi'an, Shaanxi, 710049, China

ARTICLE INFO

Article history:
Received 15 March 2016
Received in revised form
2 May 2016
Accepted 2 May 2016
Available online 3 May 2016

Keywords:
SVOCs
Dynamic interaction
Adsorption/desorption
Airborne particles
Partition

ABSTRACT

Semivolatile organic compounds (SVOCs) can be easily adsorbed on the suspended particulate matter (PM), and the exchange of SVOCs across the air-particle interface is crucial for the determination of their exposure on human. In the present study, an airborne particle with a diameter of 2.5 μm is fully reconstructed and applied to investigate the SVOCs transport mechanism and the adsorption/desorption process. The pore size distribution of the particle is statistically estimated, based on which Knudsen and Fick diffusion mechanisms are considered. The sorption process between the adsorbed SVOCs on the element carbon (EC) and SVOCs in organic matter (OM) is performed with Langmuir-isotherm model. The effective diffusivity in particle is numerically predicted and compared with the existing empirical study. The influences of the equilibrium sorption constant and the volume fraction of organic matter and carbon on the dynamic interaction process are also explored. Results show that the effective diffusivity of the PM particle with low porosity predicted with the present model is much lower than that adopted by the Bruggeman equation. The amount of adsorbed di-2-ethyhexyl phthalate (DEHP) on EC is predominant compared with the gas phase in pores and dissolved phase in PM. The total amount of DEHP transporting from air to the PM particle is highly influenced by the equilibrium sorption constant and the volume fraction of EC. The influence of volume fraction of OM on the total amount of adsorbed DEHP is slight.

1. Introduction

Semivolatile organic compounds (SVOC) constitute important classes of indoor contaminants, which are served as additives in flame retardants, plasticizers and pesticides. Studies have proved that exposure to such compounds attributes to severe adverse health effects including toxicity in reproductive and respiratory systems of humans [1,2]. Their intake by humans can be mainly conducted through three ways, dermal contact with sources, ingestion of dust and inhalation of air and airborne particles [3]. It is reported that when the particle size is fine or ultrafine, such as PM2.5, the particle-associated SVOCs can be carried into the bloodstream directly [4]. Therefore, characterizing the exchange of SVOCs between different compartments such as gas phase and airborne particles is essential for the determination of their exposure on human.

In recently decades suspended particulate matter (PM) has been the major pollutant due to the combustion of fossil fuels [5]. The main chemical components of PM include organic matter (OM), element carbon (EC) and different kinds of inorganic salts [5]. Due to the high specific surface area of PM and high solubility of SVOCs in OM, airborne particles can adsorb SVOCs easily and the interaction is a long-term process because of the low volatility of the compounds. As the particle behaviors of motion, transport and deposition are quite different for different particle sizes, the exchange of SVOCs between gas phase and PM tends to be very complicated. Liu et al. [6] pointed out that the particle-associated SVOCs behaviors are related with the size distribution of particles, and which can be directly influenced by the mass transfer limitations and the ratio of the equilibrium and residence time of the particles. Therefore, much attention has been devoted to the interaction between gas phase SVOCs and PM.

The detailed exchange process of SVOCs between the gas phase and PM can be described as illustrated in Fig. 1, where an elemental volume of PM is supposed to be a sphere with porous structure. SVOCs in air diffuse into the pore of PM and dissolute into OM.

* Corresponding author.
E-mail address: wqtao@mail.xjtu.edu.cn (W.-Q. Tao).

http://dx.doi.org/10.1016/j.buildenv.2016.05.002
0360-1323/

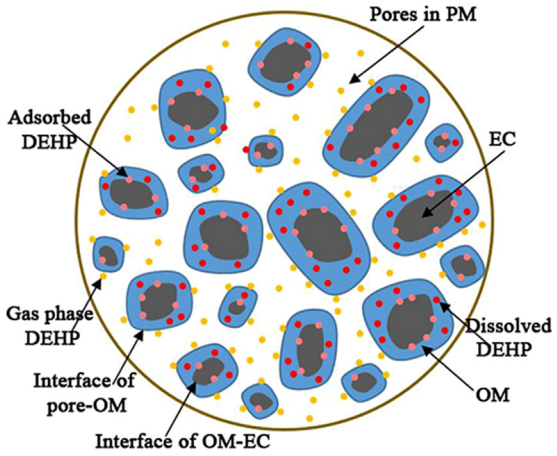

Fig. 1. Representative of physical diffusive model of DEHP in PM.

Diffusion mechanisms of SVOCs in pores may vary from Fick diffusion to Knudsen diffusion according to the pore size. When the SVOCs transfer to the interface between OM and EC, the adsorption/desorption process occurs. The mass exchange of SVOCs between dissolved and adsorbed SVOCs has been suggested by first order sorption models, among which Langmuir-isotherm model [7] and Freundlich model [8] are widely adopted. Therefore, three different phases of SVOCs exist in the PM, namely, gas, dissolved and adsorbed phase.

The existing and commonly used models to describe the interaction between gas phase and PM can be categorized as two classes. One is based on the equilibrium partition theory model assuming the adsorption and absorption being in equilibrium. The distribution of SVOCs in gas phase and PM is obtained with an equilibrium partition constant, K_p, which is related with the liquid vapor pressure and determined experimentally [9]. Details concerning K_p are reviewed in several studies [1,9–12]. However, the equilibrium state can hardly be reached if the air exchange rate is high, and therefore deviation has been observed when compared with the experimental work [11,13]. The other one is based on the dynamic mass transfer process. Rounds and Pankow [14] proposed a radial diffusion model which considers the PM consisting of a solid carbon core covered by a liquid-like organic layer. Diffusion and partition processes take place within the organic layer and the interface between carbon and OM, respectively. The model was improved later by Pankow [10] who included the external mass transfer into the model. Comparison of time scales between the internal diffusion and external mass transfer processes has been performed by Weschler and Nazaroff [11], and the result suggested that the external mass transfer process is predominant for the rate-limiting process for partition. Based upon the assumption, PM could be treated as a compartment with well-mixed SVOCs [2–4,6,15–17]. Liu et al. [15] presented a more detailed analysis on the criterion to judge the dominant factor between the internal and external mass transfer process. However, the accuracy of the model is highly dependent on the adopted mass transfer coefficient and K_p. Parameter uncertainties on K_p studied by Salthammer and Schripp [12] suggested that the calculated distribution behavior might be strongly influenced by singular value such as the vapor pressure, volume fraction of organic matter and total suspended particle. And the external mass transfer coefficient spans several orders of magnitude in the literature [16].

The above mentioned models have been adopted on the prediction of the transport and distribution of indoor SVOCs. However, the detailed morphology characteristics of the PM, such as the specific surface area, structure and pore size distribution (PSD) could hardly be considered [16]. Typically, the pore size spans several order magnitude ranging from the nano-pore to macro-pore, and the diffusion mechanism varies from Knudsen to Fick diffusion. Such a situation is obviously not satisfactory for deeply understanding the physical process and more accurately prediction. The objective of the present study is to provide a pore-scale simulation on the dynamic interaction of SVOCs and PM2.5. A more sophisticated model will be proposed which can provide a detailed SVOCs transport mechanism in PM including the particle-gas partition, mass transport and adsorption/desorption processes. As a typical kind of SVOCs, di-2-ethyhexyl phthalate (DEHP) has been chosen in this work.

In the following section, we firstly present the detailed reconstruction process of microstructures of the PM2.5, followed by the introduction to simulation model and numerical methods. Then, the detailed numerical results and discussions are presented. Finally, some conclusions are drawn.

2. Reconstruction of microstructures of the PM2.5 particle

The final chemical compositions of PM are strongly dependent upon some factors including the anthropogenic and natural sources [5]. For example, for the emissions in automobile exhaust and wood smoke, experimental study has found that the mass fractions of OM and EC of the total particulate mass are 80% and 50%, respectively [18]. Such discrepancies exhibit spatially and seasonally. Cao et al. [5] investigated the chemical compositions of winter and summer PM2.5 in fourteen Chinese cities. It is indicated that OM and EC present maximum in winter and minimum in summer. The OM concentrations in all cities vary from 13.3 to 95.8 $\mu g\ m^{-3}$ while the EC concentrations vary from 4.6 to 21.5 $\mu g\ m^{-3}$.

The microstructures of PM particles have been extensively investigated with the scanning electron microscopy (SEM) to determine the PSD and PM particles morphology [19,20]. Fig. 2 illustrates a representative SEM image of a carbonaceous particle agglomeration with its diameter around 10 μm shown by Ancelet et al. [19]. It can be found that the PM particle is a porous medium with its compositions such as OM and EC filling in the pores, and the PSD is at nanoscale. Although the specific microstructures and chemical compositions of PM particles may differ greatly, our focus is mainly on the general characteristics of the pore-scale process of DEHP transferring in OM and pore and adsorption/desorption process at EC surfaces. Such general characteristics can be obtained by selecting some typical values of the volume fractions of OM and EC and the porosity of PM particles. According to the experimental

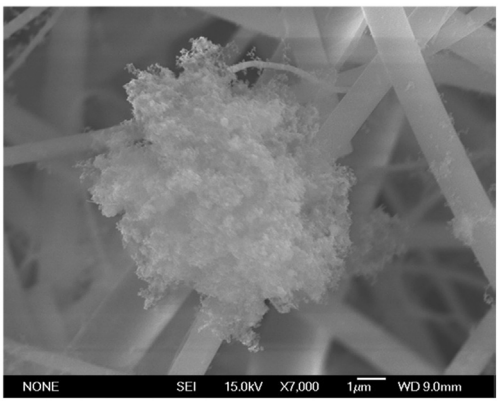

Fig. 2. SEM of a representative carbonaceous particle (reproduced from Ancelet et al. [19]).

data given by Cao et al. [5], the basic case we choose for the above three values are 0.3, 0.3 and 0.4, respectively.

The microstructure of a PM particle can be obtained via computational reconstruction algorithms [21,22] by lattice Boltzmann method (LBM) [23,24]. The D3Q19 model is adopted here for the 3D generation. The quartet structure generation set (QSGS) proposed by Wang et al. [22] is employed in this paper. The reconstruction of a PM particle is implemented by reconstruction of EC and OM in a small space (particle) to their specified volume fraction. The procedures for the reconstruction of EC are briefly introduced as follows: (1) EC seeds are firstly randomly assigned according to a distribution probability, c_d. A higher c_d represents more seeds in the computational domain, and therefore the EC agglomerates are bigger. $c_d = 0.01$ was chosen in the present study; (2) The existing seeds grow to the neighboring cells along the directions shown in Fig. 3. The growth probabilities for the directions of 1,2,3,4,5,6 are α and those for the rest directions are $\alpha/2$ ($\alpha = 0.05$ in the present study); (3) Repeat step (2) until the pre-specified volume fraction of EC is achieved. The growth of OM is a little different from that of EC: (1) All the existing seeds of EC are initially served as the seeds for the growth of OM; (2) The existing seeds grow to the neighboring cells when the neighboring cells are not marked as EC cells; (3) Repeat step (2) until the pre-specified volume fraction of OM is obtained.

In the present study, a PM2.5 particle surrounded in gas phase DEHP was studied. To save the computational resources, one-eighth PM2.5 particle was chosen and reconstructed in Fig. 4 according to the basic case introduced above. Parameter sensitivities on the OM and EC are performed via varying the volume fractions of OM and EC. The sizes of the computational domain are $1.5 \times 1.5 \times 1.5$ μm. The mesh system adopted is $150 \times 150 \times 150$, with the mesh resolution of 10 nm. Detailed information on the structures will be discussed in Section 4.

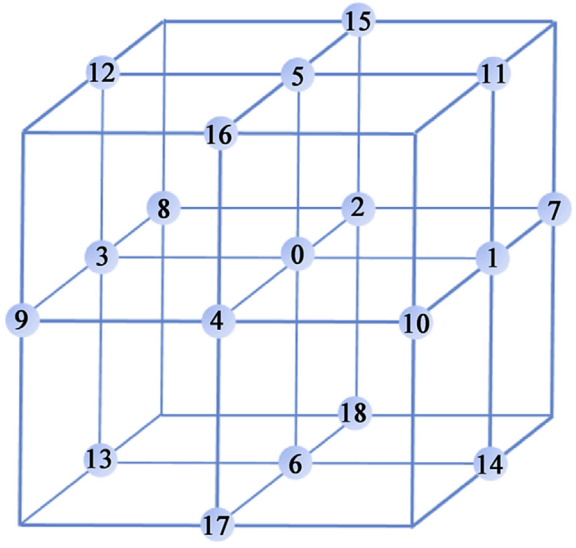

Fig. 3. Cell growing directions in the QSGS or the D3Q19 model in LBM.

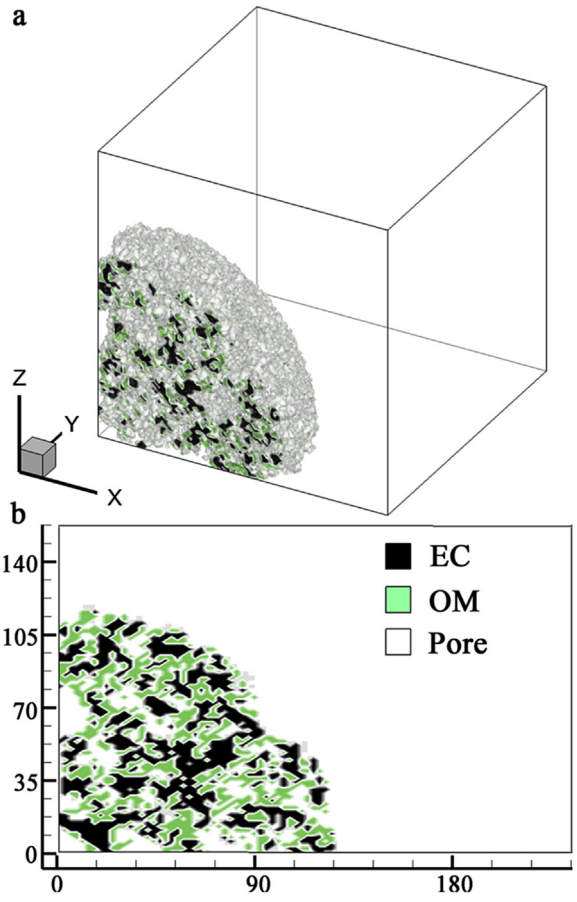

Fig. 4. Reconstructed nanostructures of a one-eighth PM2.5, (a) 3D structure; (b) Detailed distributions of EC, OM and pore at the cross-section of y = x.

3. Simulation model and numerical methods

3.1. Governing equations

Following the work presented by Weschler and Nazaroff [11] and Liu et al. [15], the convection effect on DEHP diffusion in the PM particle is neglected. The DEHP transport equation in pores can be described by Eq. (1), where C is the gas phase concentration and D_b is the diffusivity.

$$\frac{\partial C}{\partial t} = \nabla \cdot (D_b \nabla C) \tag{1}$$

In the pores, bulk diffusion and Knudsen diffusion are included according to the pore diameter. The Knudsen diffusivity D_{Kn}, is calculated as

$$D_{Kn} = \frac{d_p}{3}\sqrt{\frac{8RT}{\pi M_{DEHP}}} \tag{2}$$

where R is the universal gas constant, T is the temperature, M_{DEHP} is the molecular weight of DEHP, d_p is the pore diameter. The critical pore diameter to distinguish the macro-pore from meso-pore is defined as ten times of the molecular free path λ of DEHP [25]. The diffusivity in macro-pore is denoted as D_b, while that in meso-pore is calculated with $\left(D_b^{-1} + D_{Kn}^{-1}\right)^{-1}$ [25]. d_p is locally calculated via the 13-direction averaging method [26].

When DEHP transports to pore-OM interface, it will be dissolved in OM. The dissolved DEHP concentration at the interface C_e is determined by partition coefficient as described in Eq. (3).

$$C_e = K_P C \tag{3}$$

The DEHP diffusion in OM is described as follows

$$\frac{\partial C_e}{\partial t} = \nabla \cdot (D_e \nabla C_e) \tag{4}$$

where D_e is the DEHP diffusivity in OM. Then, DEHP will be adsorbed on the EC and the whole process is assumed to follow the Langmuir-isotherm model. All the relevant parameters in the model are listed in Table 1. By altering the relevant parameters in this table, the present model can also be applied to other kinds of SVOCs.

3.2. Initial conditions and boundary conditions

The DEHP concentration in PM is initially assumed to be zero while the gas phase DEHP in the computational domain with PM excluded is C_0. Constant DEHP concentration C_0 is fixed on the top, right and forward sides of the domain, while symmetrical conditions are applied on the other sides of the domain. At the interface of OM-EC, Langmuir-isotherm condition is defined [26].

$$\begin{aligned} \frac{\partial C_e(x,t)}{\partial t} &= L(-k_a C_e(x,t) + k_d M(x,t)) \\ \frac{\partial M(x,t)}{\partial t} &= k_a C_e(x,t) - k_d M(x,t), k_e = \frac{k_a}{k_d} \end{aligned} \tag{5}$$

where k_a is the adsorption constant, k_d is the desorption constant, k_e is the equilibrium sorption constant and L is the loading ratio which equals to the mesh resolution in the present study. The adsorbed DEHP at the location of $\mathbf{x}$ and time t is denoted as $M(x,t)$. The detailed implementation process of the Langmuir-isotherm boundary can be found in our previous work [26].

3.3. Numerical methods

Due to its simplicity and flexibility in dealing with complex boundary conditions, LBM has been applied to simulate the whole DEHP transport process in PM particle. Unlike directly solving the partial differential equations (Eq. (1)–(4)), the diffusion of DEHP can be described by a set of species distribution functions as a collective behavior of pseudo-particles on a mesoscopic level. The simpler and popular BGK collision operator is adopted

$$f_i(\mathbf{x} + \Delta\mathbf{x}, t + \Delta t) - f_i(\mathbf{x}, t) = -\frac{1}{\tau}\left(f_i(\mathbf{x}, t) - f_i^{eq}(\mathbf{x}, t)\right) \tag{6}$$

where $f_i(\mathbf{x}, t)$ is the species distribution function at the lattice site $\mathbf{x}$ and time t, τ is the dimensionless relaxation time, $\Delta\mathbf{x} = c\mathbf{e}_i\Delta t$ with c, $\Delta\mathbf{x}$ and Δt as the lattice speed, space and time step, respectively. For a three-dimensional space with nineteen velocities at a given position D3Q19, the discrete velocities $\mathbf{e}_i$ are given by

Table 1
Parameter values used for the basic case in the simulation [15,16].

Parameter	Value
Adsorption rate constant, k_a	1.0 m h^{-1}
DEHP diffusivity in air, D_b	2.64×10^{-6} m^2 s^{-1}
Desorption rate constant, k_d	10^7 h^{-1}
DEHP diffusivity in OM, D_e	1.78×10^{-9} m^2 s^{-1}
Initial concentration of DEHP, C_0	0.65 μg m^{-3}
Partition coefficient, K_p	$10^{12.9}$
Molecular weight of DEHP, M_{DEHP}	390.56 g mol^{-1}
Temperature, T	298.0 K
Volume fraction of EC, f_{EC}	0.3
Volume fraction of OM, f_{OM}	0.3

$$\mathbf{e}_i = \begin{cases} 0 & i = 0 \\ (\pm1,0,0),(0,\pm1,0),(0,0,\pm1) & i = 1-6 \\ (\pm1,\pm1,0),(0,\pm1,\pm1),(\pm1,0,\pm1) & i = 7-19 \end{cases} \tag{7}$$

The corresponding equilibrium distribution functions $f_i^{eq}(\mathbf{x}, t)$ are given by

$$f_i^{eq}(\mathbf{x}, t) = \begin{cases} C/3 & i = 0 \\ C/18 & i = 1-6 \\ C/36 & i = 7-19 \end{cases} \tag{8}$$

The concentration $C(C_e)$ and diffusivity $D_{DEHP}(D_{DEHP,e})$ can be obtained as follows:

$$C(C_e) = \sum_i f_i(\mathbf{x}, t) \tag{9}$$

$$D(D_e) = \frac{1}{3}\left(\tau(\tau_e) - \frac{1}{2}\right)\frac{\Delta\mathbf{x}^2}{\Delta t} \tag{10}$$

With Chapman-Enskog expansion, Eqs. (6) and (9) can be recovered to Eqs. (1) and (4). The code is parallelized using Message Passing Interface (MPI) on 300 CPU cores. The running time to reach an equilibrium state for the basic case is about 5 days.

4. Results and discussion

4.1. Characterization of the PM particle structures

The characteristics of the PM particle microstructures including the PSD and specific surface area determine the critical transport properties and adsorption/desorption process in the PM. By calculating the pore diameter of each cell in the domain, the PSD can be statistically obtained. In the following discussion, the basic case listed in Table 1 is taken as an example. Fig. 5 shows the PSD of the reconstructed PM particle. The minimum pore size captured in this study is 10 nm due to the resolution of the mesh. All the pore diameters are in the range of 10–130 nm, indicating the nanoscale characteristic of the PM particle. The majority of the pore diameters are around 10 λ, and only a small amount of pore diameters is larger than 100 nm. The distribution characteristic of the pore diameters qualitatively agrees well with the existing studies [26,27]. Besides, according to the statistical results, 54% of the pores are at meso-scale, in which the diffusion mechanism of DEHP is Knudsen and Fick diffusion. Therefore, the effective diffusivity of the PM particle

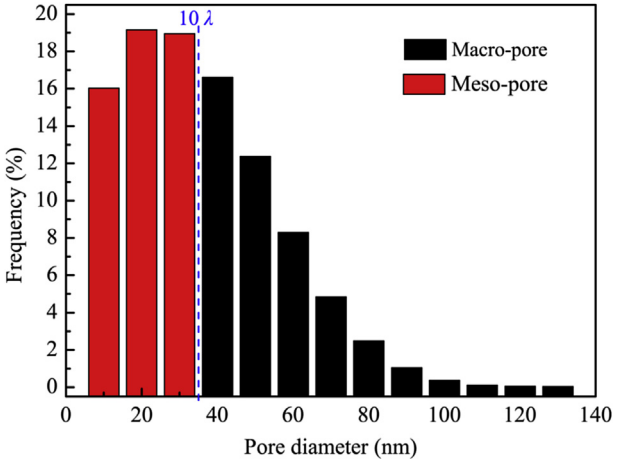

Fig. 5. PSD of the reconstructed PM.

is essentially dependent on the PSD, which will be discussed later.

The total cell volume for EC and OM are 166822 and 166762 $(\Delta \mathbf{x})^3$, respectively. Meanwhile, the total surface area of EC and OM are 147526 and 161001 $(\Delta \mathbf{x})^2$, respectively. The total surface area for EC is smaller than that for OM. The reason is mainly attributed to their different states that EC is in agglomerate state while OM is in film state. The specific surface area is determined by the cell resolution $\Delta \mathbf{x}$ that higher resolution results in higher specific surface area. With $\Delta \mathbf{x}$ equals 10 nm and the density of PM is 10^6 g m^{-3} [15], the specific surface area of OM and EC are 96.5 and 88.5 m^2 g^{-1} for the PM shown in Fig. 4, respectively. A high surface area of OM could promote the dissolution of DEHP in gas phase, while a high surface area of EC could increase the total amount of adsorbed DEHP.

4.2. Effective diffusivity

To validate our self-developed code of the reconstruction method, the effective diffusivity of DEHP in a cubic domain containing different volume fractions of EC and OM is numerically predicted and compared with the existing results. For this verification a domain of 1 × 1 × 1 μm, is adopted and discretized by 100 × 100 × 100 lattices. The cells in the domain are labeled 0, 1 and 2 representing pore, EC and OM, respectively. Diffusivities in different kinds of cells, especially for the meso-/macro-pores, are assigned according to the discussion in Section 3.1.

Comparison of the effective diffusivity obtained with the present model and several existing work [27,28] is plotted in Fig. 6. The effective diffusivity is normalized by the bulk diffusivity listed in Table 1. Since the PSDs generated with the present stochastic reconstruction method may be different within a certain range [26], each value shown in Fig. 6 is statistically averaged by five different cases to minimize the random error. The porosity is changed only by altering the volume fraction of OM (referred as mode 1) or EC (referred as mode 2) while keeping the volume fraction of the other composite a constant. As the porosity increases, the sum of the volume fraction of OM and EC decreases, and therefore the effective diffusivity increases. The result predicted with the present model agrees well with Lange et al. [28], while a bit higher than that given by Chen et al. [27]. The discrepancy might be attributed to the following reasons. As the mesh resolution adopted in the work of Chen et al. [27] is much smaller than the present study, the percentage of meso-pores is higher. Due to a smaller diffusivity in meso-pore than that in macro-pore, the effective diffusivity in our work is higher. Besides, there are three components involved in our model, and OM is permeable with a given diffusivity. The solid phase in the work of Chen et al. [27] is impermeable, which explains a higher effective diffusivity predicted with our model. It can also be found in Fig. 6 that the variation tendency of effective diffusivity under two different modes is different. The effective diffusivity with $f_{OM} = 0.3$ increases with porosity faster, especially at a higher porosity, and it is mainly due to a higher volume fraction of OM under the same porosity. For example, when the porosity is 0.3, the volume fraction of OM under mode 1 is 0.4, and therefore the effective diffusivity in mode 1 is higher than that in mode 2.

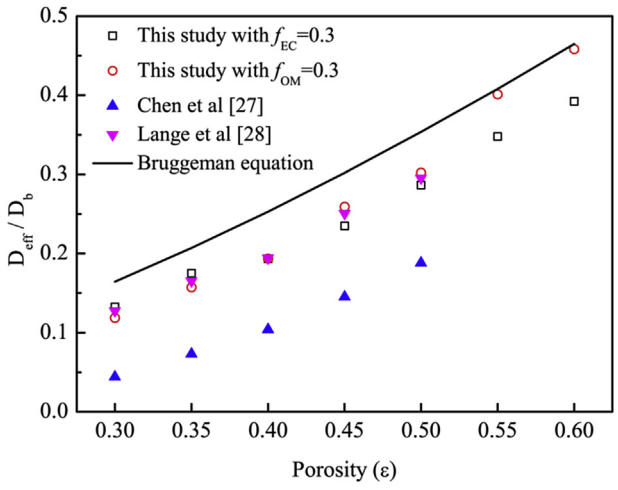

Fig. 6. Variations of effective diffusivity with different porosities.

In Fig. 6, the effective diffusivity calculated with Bruggeman equation is also included, which is obtained with the following equation:

$$D_{\text{eff}} \big/ D_{\text{b}} = \frac{\varepsilon}{\tau} \tag{11}$$

where ε and τ are the porosity and tortuosity of a porous medium, respectively. The tortuosity τ, representing the ratio between the actual flow path length and the straight length of a porous medium, is usually set as $\tau = \varepsilon^{-0.5}$. It is shown in Fig. 6 that the effective diffusivity predicted with Bruggeman equation is overestimated. This may be explained as follows. With Knudsen diffusivity considered, the total diffusivity in the local meso-pore is smaller. For example, under the simulation condition of $T = 293$ K and $P = 1$ atm, the Knudsen diffusivity of DEHP in a pore size of 10 nm is 4.24×10^{-7} m^2 s^{-1}, and therefore the total diffusivity is 3.65×10^{-7} m^2 s^{-1}, which is much smaller than D_b. Moreover, the irregular model generated may lead to a higher tortuosity, which is also confirmed by several studies [26,29].

4.3. DEHP distribution features in three different phases

In order to gain a direct impression of the transport process of DEHP, simulation results for the basic case are presented in Fig. 7. Four different cross-sections along the x-direction are selected. It can be seen that as time proceeds DEHP amount in three different phases increases and then reaches a steady state. Fig. 7(a) shows the DEHP in gas phase. Since DEHP concentration in air is initially set as C_0 and that in the PM is set as 0, DEHP transports greatly from air to the pores in PM particle owing to the large concentration gradient. With more DEHP diffuses into the PM particle, the variation of DEHP concentration tends to be slower. Besides, one part of the gas phase DEHP will partition at the interface of OM-pore and dissolve into OM. Compared with the transport process in OM, DEHP transports easily in the pores due to its relatively high diffusivity. The diffusivity in pores is several orders magnitude higher than that in OM. It can also be found that unlike the cross-section of P4, the transport resistance for P1 is high, and therefore the time needed to reach a steady state is comparatively longer.

Fig. 7(b) presents the distribution of dissolved DEHP in OM. Dissolved DEHP is highly related with gas phase DEHP in pores, since the concentration of dissolved DEHP at the interface of OM-EC is determined by K_p and the concentration of gas phase DEHP (see Eq. (3)). The dissolved DEHP in OM diffuses relatively slowly because of its small diffusivity. As EC is covered by OM, when the dissolved DEHP diffuses to the interface of OM-EC, the dissolved DEHP will be adsorbed at the EC surfaces.

Fig. 7(c) displays the distribution of adsorbed DEHP on EC surfaces. The concentration of adsorbed DEHP highly depends on the concentration of dissolved DEHP in OM and the adsorption/desorption rate constants (see Eq. (5)). Since the adsorbed DEHP is initially set as 0, its concentration may increase sharply at

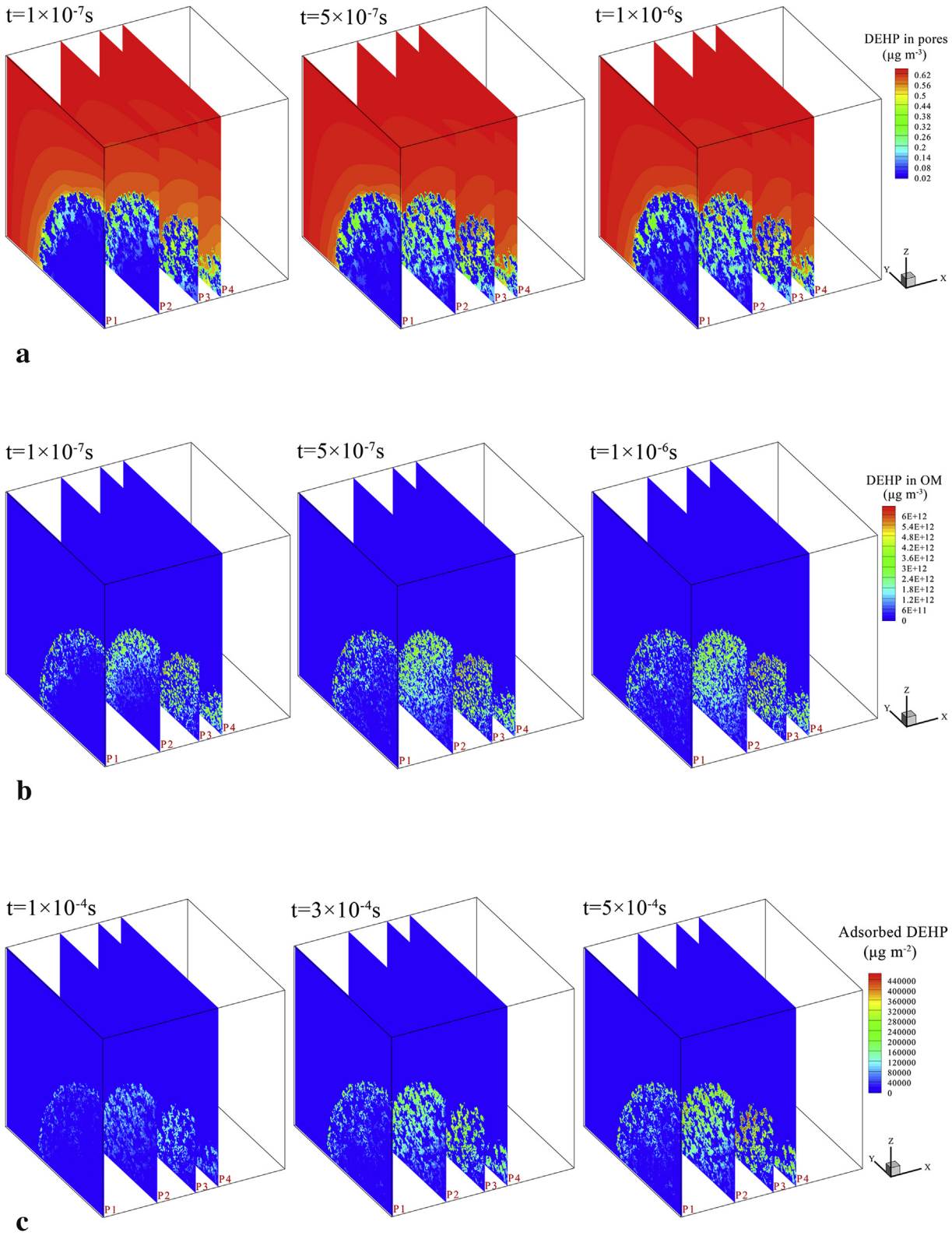

Fig. 7. DEHP distribution in different phases: (a) gas phase DEHP in pores; (b) dissolved DEHP in OM; (c) adsorbed DEHP in OM-EC surfaces.

beginning since the amount of DEHP desorbed can be neglected. When the adsorbed and desorbed DEHP at the EC surfaces are the same, an equilibrium state between the dissolved and adsorbed DEHP is reached. Finally, all the phases of DEHP in PM particle will obtain a steady state. According to the present study, the time needed for the adsorbed DEHP reaching a steady state is significantly longer than that for the other two phases. It takes about 10^{-3} s for the adsorbed DEHP while 10^{-6} s for the other two phases

to reach an equilibrium state. The total amount of the adsorbed, dissolved and gas phase DEHP in the PM particle at the equilibrium state is 4.842×10^{-6}, 5.426×10^{-7} and 6.968×10^{-20} μg, respectively. The result indicates that the majority of DEHP is mainly adsorbed at the EC surfaces and the DEHP diffused in gas phase can be neglected when compared with the other two phases. The factors influencing the total amount of DEHP include the morphology of the PM particle (such as the porosity, aspect ratio, volume fraction of EC and OM) and the equilibrium sorption constant. In the following studies on the effects of equilibrium sorption constant, volume fractions of EC and OM on the transport process of DEHP will be presented.

It is worth noting that from the amounts of the three phases, the effective partition coefficient can be predicted as follows. The total amount of DEHP in PM2.5 can be calculated as:

$$m_{\text{total}} = m_{\text{Dissoluted}} + m_{\text{Absorbed}} + m_{\text{Gas}} \tag{12}$$

where $m_{\text{Dissoluted}}$, m_{Absorbed} and $m_{\text{Gas}}$are the amount of DEHP in adsorbed, dissolute and gas phase, respectively. The effective partition coefficient $K_{\text{P,eff}}$ can be obtained with the following equation:

$$K_{\text{P,eff}} = \frac{m_{\text{total}}}{1/8\pi r^3} \Big/ C_0 \tag{13}$$

And the gas/particle partition coefficient K_{part} (μg m^{-3}) can be calculated by

$$K_{\text{part}} = K_{\text{P,eff}} \Big/ \rho_{\text{part}} \tag{14}$$

with an appropriate value of particle density ρ_{part}.

4.4. Effect of the equilibrium sorption constant

Since the equilibrium sorption constant is a crucial factor which affects the mutual conversion between the adsorbed and dissolved DEHP directly, parameter sensitivity analyses are performed to examine its influence on the DEHP transport process in PM particle. By comparing a set of adsorption/desorption rate constants while keeping the equilibrium sorption constant the same, Guo [16] investigated the adsorption characteristics for PM2.5 particle and concluded that the total amount of DEHP is only determined by the equilibrium sorption constant while the time needed to reach a steady state shortens greatly with the increasing of adsorption/desorption rate constants. By introducing Langmuir-isotherm model to the VOC adsorption/desorption process of building material, similar results that the equilibrium state is influenced by adsorption/desorption rate constant can be found in the study of Mu et al. [26]. Typically, there are two modes to change the equilibrium sorption constant. One is by altering the desorption rate constant while the other is by altering the adsorption rate constant. According to references [16,26], the amount of VOCs/SVOCs adsorbed is only influenced by the equilibrium sorption constant, and therefore there is no need to investigate the influence of adsorption rate constant and desorption rate constant separately. In this study, the equilibrium sorption constant is changed only by altering the desorption rate constant while fixing the adsorption rate constant for simplicity. Fig. 8 depicts the time evolution of DEHP in different phases with different equilibrium sorption constants. As is shown in Fig. 8(a), the DEHP concentrations in gas phase and DEHP amount in OM increase sharply and then reach a steady state in a short time (less than 1×10^{-6} s). It is interesting that there is no significant discrepancy for DEHP in gas phase and dissolved phases under orders-different equilibrium sorption

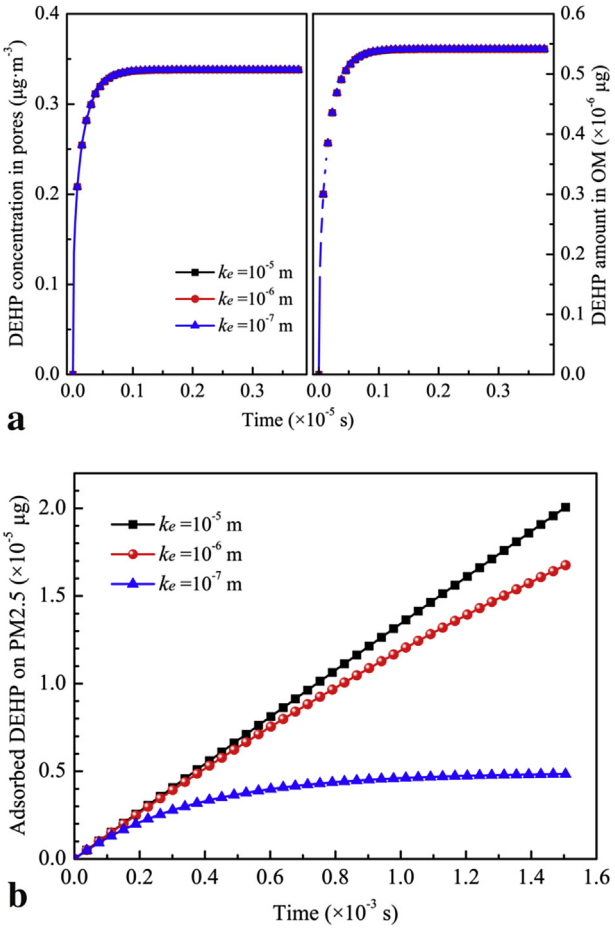

Fig. 8. Time evolution of DEHP in different phases with different equilibrium sorption constants: (a) adsorbed DEHP; (b) dissolved DEHP in OM and DEHP concentration in pores.

constants. The reason can be explained as follows. For the dissolved DEHP transferring to the interface of OM and EC it is required a rather longer time than that for the DEHP in air diffusing to the pores in PM particle, therefore, during the period of 0–1×10^{-6} s, the variation of DEHP concentration will not be affected by the equilibrium sorption constants. Attention is now turned to the adsorbed DEHP, the desorption rate of DEHP from the EC surfaces is small during this period. Therefore, the net adsorption rate of DEHP at the EC surfaces will not be influenced. The result is supported by Fig. 8(b) that the amount of adsorbed DEHP during this period is comparatively small when compared with the amount at steady state.

In Fig. 8(b) it is presented that the adsorbed DEHP at the EC surfaces increases with time under different equilibrium sorption constants. It can be found that the total amount of adsorbed DEHP varies linearly and then decreases until a steady state is reached. For example, as the equilibrium sorption constant is 10^{-7} m, the adsorbed DEHP is little and therefore the second term in the right side of Eq. (5) can be neglected. When the adsorbed DEHP increases to some extent, the DEHP desorbed from the EC surfaces tends to be significant. As is stated before, higher equilibrium sorption constant corresponds to a lower desorption rate constant (see Eq. (5)), therefore the time needed for the desorbed DEHP from the EC surfaces increases greatly with a higher equilibrium sorption constant. Meanwhile, a higher equilibrium sorption constant will result in a higher adsorbed DEHP concentration at the EC surfaces. Based

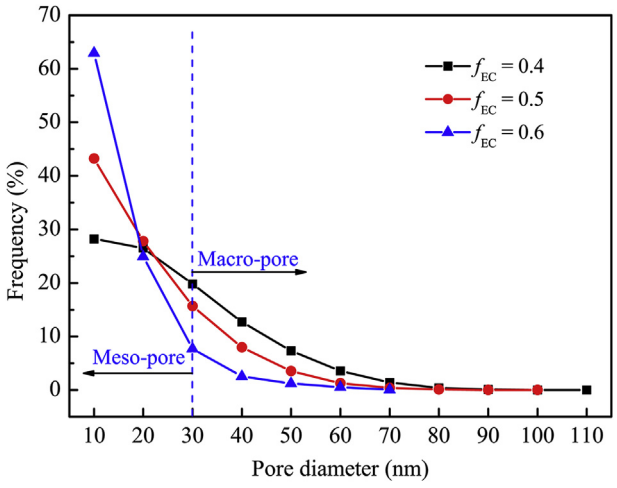

Fig. 9. PSD distributions with different volume fractions of EC.

on the present study, it can be concluded that the total amount of DEHP transporting from air to PM depends on the equilibrium sorption constant significantly, and the time needed to reach an equilibrium state is mainly determined by the adsorption/desorption process other than the DEHP diffusing in OM.

4.5. Effect of the volume fraction of EC

The morphology of PM2.5 particle, characterized by several parameters such as porosity, PSD, tortuosity and aspect ratio, is affected by the volume fraction of EC greatly. Therefore, the transport of DEHP in pores and the adsorption/desorption process will be influenced by this factor. Fig. 9 shows the PSD distributions under different volume fractions of EC (f_{EC}). As f_{EC} increases, the porosity of the PM particle decreases, and therefore the maximum pore diameter decreases. For example, the maximum pore diameters with f_{EC} equaling 0.3 (see Fig. 5), 0.4, 0.5 and 0.6 are 130, 110, 100 and 70 nm, respectively. Meanwhile, the frequency of meso-pores increases significantly with the increase in f_{EC}, which will result in lower effective diffusivity of DEHP in pores. For the particle studied as f_{EC} equals 0.4, 0.5 and 0.6, the specific surface areas of OM/EC are 96.2/83.0, 95.4/75.9 and 93.4/67.9 $m^2\ g^{-1}$, respectively. Note that a higher specific surface area of OM benefits the transport of dissolved DEHP since f_{OM} is the same. Despite the specific surface area for EC is lower with a higher f_{EC}, the total surface area is higher and therefore benefits the increases of total amount of adsorbed DEHP.

Fig. 10 presents the time evolution of DEHP in different phases. As shown in Fig. 10(a), the time needed for the gas phase DEHP in pores to reach a steady state decreases and the concentration at steady state increases with the reduction of f_{EC}. Similar result has been found for the dissolved DEHP in OM. The adsorbed DEHP at the EC surfaces is illustrated in Fig. 10(b). It can be seen that the

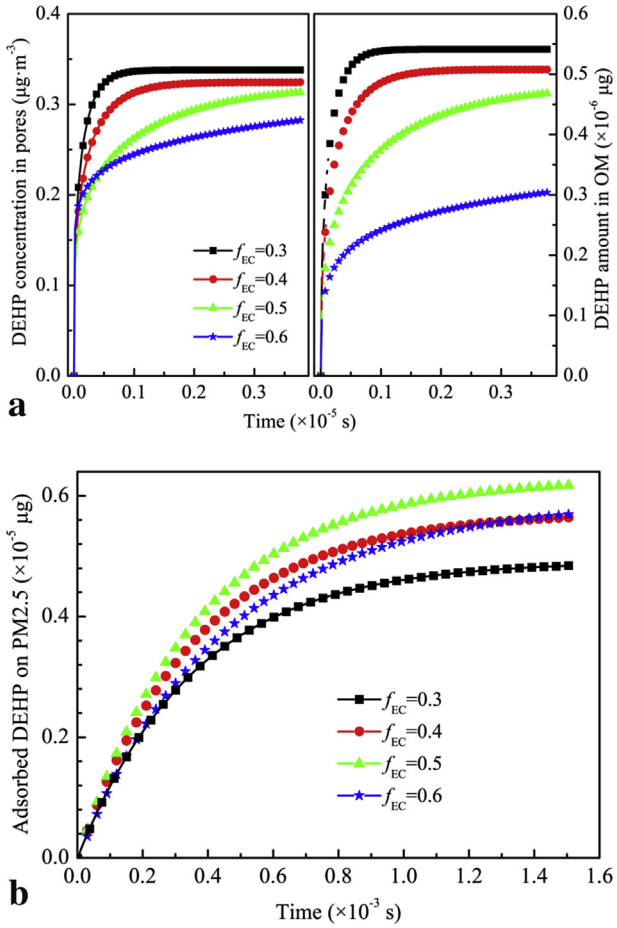

Fig. 10. Time evolution of DEHP in different phases with different volume fractions of EC: (a) dissolved DEHP in OM and DEHP concentration in pores; (b) adsorbed DEHP.

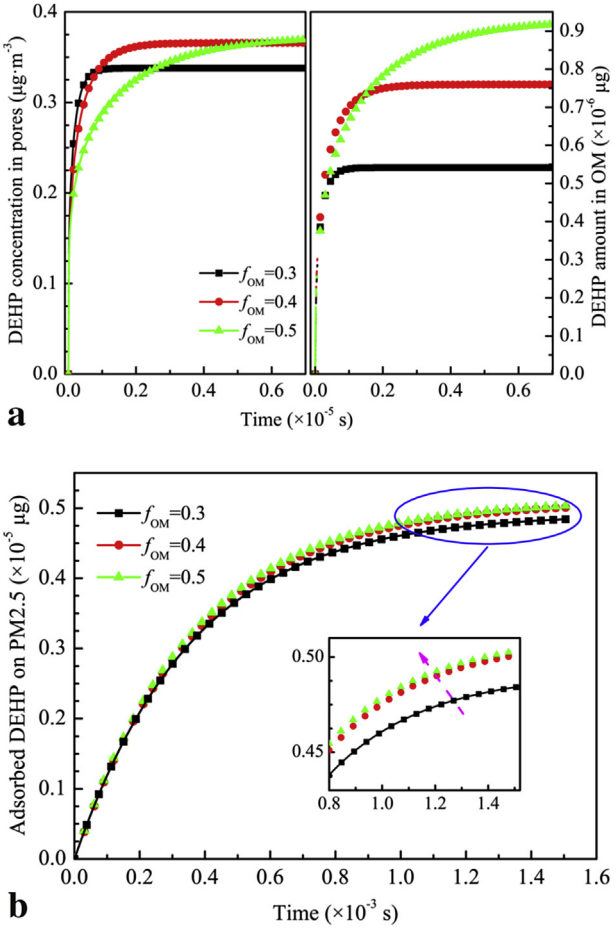

Fig. 11. Time evolution of DEHP in different phases with different volume fractions of OM: (a) dissolved DEHP in OM and DEHP concentration in pores; (b) adsorbed DEHP.

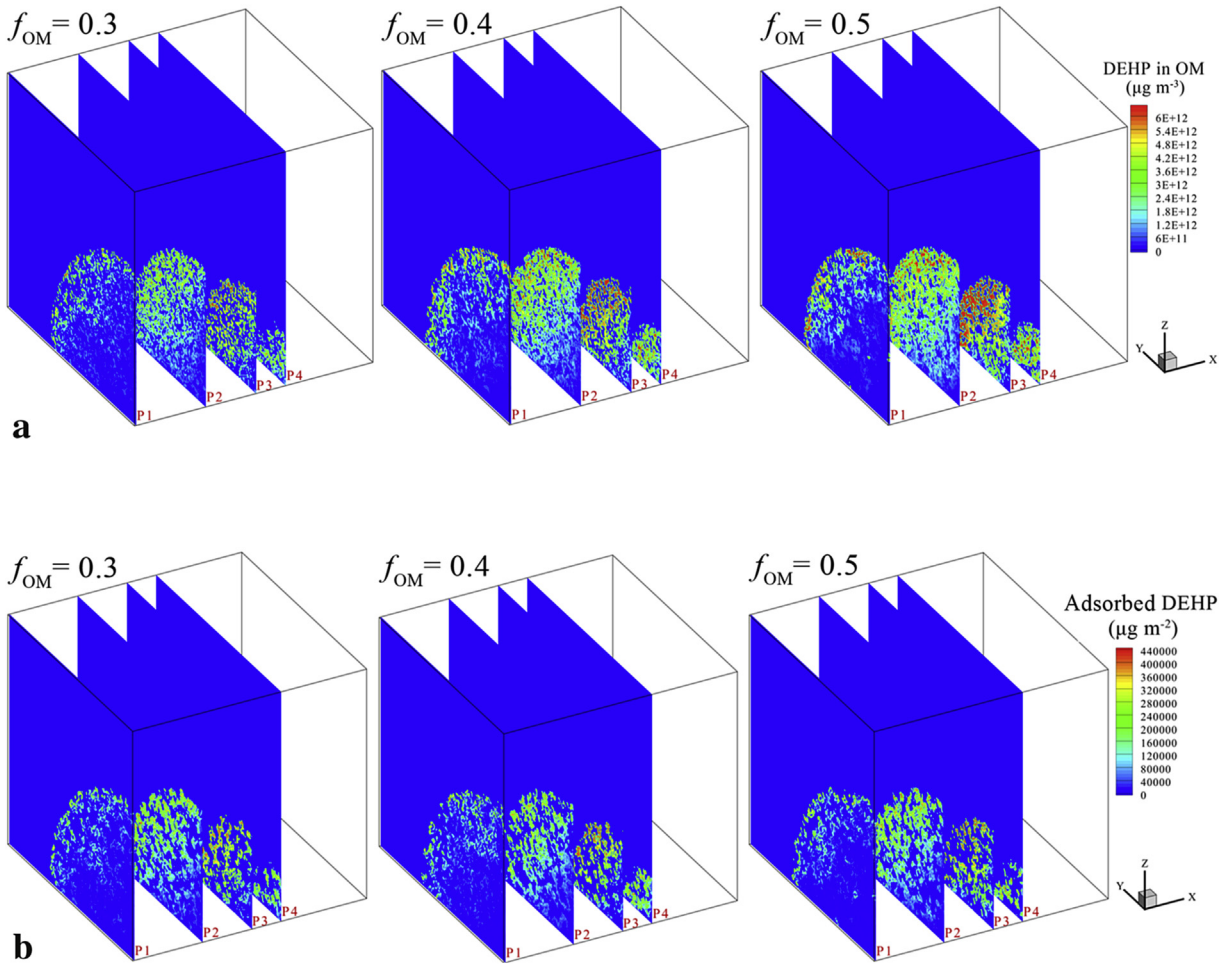

Fig. 12. DEHP distribution in different phases with different volume fractions of OM at t = 4 × 10^{-4} s: (a) dissolved DEHP in OM; (b) adsorbed DEHP at OM-EC surfaces.

adsorbed DEHP of different f_{EC} is almost the same at the very beginning (during the period of 0–5 × 10^{-5} s). As the total area for adsorption/desorption at the EC surfaces increases with f_{EC}, while the dissolved DEHP decreases with f_{EC}, and therefore no significant discrepancy exists. As time proceeds, the dissolved DEHP in OM reaches a steady state, the variation of adsorbed DEHP is highly depends on the equilibrium concentration of dissolved DEHP ($C_{e,equil}$). When f_{EC} is lower than 0.6, the difference of $C_{e,equil}$ among the cases in the present study is relatively small, and therefore the variation of the adsorbed DEHP depends highly on the total surface of EC. When f_{EC} equals 0.6, $C_{e,equil}$ is comparatively small. A tradeoff between the increasing total surface area and decreasing $C_{e,equil}$ results in a lower adsorbed DEHP. Therefore, it can be concluded that the equilibrium adsorbed DEHP increases and then decreases with f_{EC} based on the total surface area of EC and the equilibrium dissolved DEHP in OM.

4.6. Effect of the volume fraction of OM

The volume fraction of OM (f_{OM}) can affect the diffusion of dissolved DEHP in OM, and therefore influences the adsorption/desorption process at the interface of OM-EC. Fig. 11 presents the time evolution of DEHP in different phases with different volume fractions of OM. As shown in Fig. 11(a), with the increase of f_{OM}, the concentration of DEHP in pores reaches an equilibrium state much faster. This is mainly because the effective diffusivity decreases with the decrease of porosity. It is interesting to find that the concentration of DEHP in gas phase increases with f_{OM}. The reason may be explained as follows. The diffusivity of DEHP in OM is several orders lower than that in pores, therefore, OM can be regarded as resistance for the gas phase DEHP transporting to OM, which in turn benefits the accumulation of gas phase DEHP in pores. However, the increase of OM can hinder the DEHP transporting from air to the pores in the PM particle. The increment of DEHP in gas phase becomes less with the increase of f_{OM}. From Fig. 11(a), it can also be expected that the total amount of dissolved DEHP in OM increases with f_{OM}.

The evolution of adsorbed DEHP at the EC surfaces is illustrated in Fig. 11(b). It can be found that the adsorbed DEHP increases with f_{OM} slightly. This may be attributed to the specific area of EC and the total amount of dissolved DEHP. With the random reconstruction method, isolated EC which is not covered by OM may exist in the PM particle. With the increase of f_{OM}, the possibility of EC covered by OM tends to be higher, which results in higher interface area between OM and EC. The interface area is considered to be the reaction surface where adsorption/desorption occurs. For example, the specific areas for EC with f_{OM} equaling 0.3, 0.4 and 0.5 are 88.5, 88.6 and 88.6 m^2 g^{-1}, respectively.

Fig. 12 shows the DEHP distribution in dissolved and adsorbed phases at t = 4 × 10^{-4} s. It can be seen that dissolved DEHP in OM increases with f_{OM} since the interface area between the pore and OM increases. The dissolved DEHP mainly distributes away from the center of PM particle. Similar distribution characteristics exist for the adsorbed DEHP. The adsorbed DEHP shows no significant

difference with different f_{OM} as is shown in Fig. 12(b).

5. Conclusions

In the present study, the dynamic interaction between DEHP and the PM particle is numerically investigated with LBM at pore-scale. The PM particle is reconstructed with QSGS method and its characteristics of structures including the specific area and PSD are statistically studied. Results show that the majority of pore in the PM particle belongs to meso-pore, and its frequency increases with the decrease of porosity. The effective diffusivity of the PM particle calculated with Bruggeman equation is much higher than that predicted with the present model, especially for the low porosity due to the Knudsen diffusion considered. The total amount of DEHP transporting from air to the PM particle mainly depends on the adsorbed DEHP at the EC surfaces other than the DEHP in gas phase and dissolved phase in OM. The equilibrium sorption constant shows no influence on the time evolution of dissolved and gas phase DEHP, while the adsorbed DEHP and the time needed to reach a steady state increase greatly with the equilibrium sorption constant. The DEHP in gas phase and dissolved phase decrease with the volume fraction of EC, while the adsorbed DEHP increases firstly and then decreases due to a tradeoff between the increasing total surface area and the decreasing $C_{e,equil}$. The total amount of dissolved phase DEHP increases with the volume fraction of OM, while the gas phase and the adsorbed DEHP increase slightly.

Acknowledgement

This work is supported by the 12th Five-Year National Key Technology R & D Program (2012BAJ02B03) and the Key Project of the National Natural Science Foundation of China (51136004).

References

[1] C.J. Weschler, W.W. Nazaroff, Semivolatile organic compounds in indoor environments, Atmos. Environ. 42 (40) (2008) 9018–9040.
[2] Y. Liang, O. Caillot, J. Zhang, J. Zhu, Y. Xu, Large-scale chamber investigation and simulation of phthalate emissions from vinyl flooring, Build. Environ. 89 (2015) 141–149.
[3] J.C. Little, C.J. Weschler, W.W. Nazaroff, Z. Liu, E.A. Cohen Hubal, Rapid methods to estimate potential exposure to semivolatile organic compounds in the indoor environment, Environ. Sci. Technol. 46 (20) (2012) 11171–11178.
[4] Q. Chen, K. Hu, Prediction model for SVOCs transport in the air and interactions with airborne particles, Atmos. Environ. 96 (2014) 61–69.
[5] J.J. Cao, Z.X. Shen, J.C. Chow, J.G. Watson, S.C. Lee, X.X. Tie, Winter and summer PM2.5 chemical compositions in fourteen Chinese cities, J. Air Waste Manage. 62 (10) (2012) 1214–1226.
[6] C. Liu, Y. Zhang, C.J. Weschler, The impact of mass transfer limitations on size distributions of particle associated SVOCs in outdoor and indoor environments, Sci. Total Environ. 497–498 (2014) 401–411.
[7] B.A. Tichenor, Z. Guo, J.E. Dunn, L.E. Sparks, M.A. Mason, The interaction of vapour phase organic compounds with indoor sinks, Indoor Air 1 (1) (1991) 23–35.
[8] M.D. Van Loy, V.C. Lee, L.A. Gundel, J.M. Daisey, R.G. Sextro, W.W. Nazaroff, Dynamic behavior of semivolatile organic compounds in indoor air. 1. Nicotine in a stainless steel chamber, Environ. Sci. Technol. 31 (9) (1997) 2554–2561.
[9] I.T. Cousins, A.J. Beck, K.C. Jones, A review of the processes involved in the exchange of semi-volatile organic compounds (SVOC) across the air-soil interface, Sci. Total Environ. 228 (1) (1999) 5–24.
[10] J.F. Pankow, An absorption model of gas/particle partitioning of organic compounds in the atmosphere, Atmos. Environ. 28 (2) (1994) 185–188.
[11] C.J. Weschler, W.W. Nazaroff, SVOC partitioning between the gas phase and settled dust indoors, Atmos. Environ. 44 (30) (2010) 3609–3620.
[12] T. Salthammer, T. Schripp, Application of the Junge- and Pankow-equation for estimating indoor gas/particle distribution and exposure to SVOCs, Atmos. Environ. 106 (2015) 467–476.
[13] Y. Xu, J.C. Little, Predicting emissions of SVOCs from polymeric materials and their interaction with airborne particles, Environ. Sci. Technol. 40 (2) (2006) 456–461.
[14] S.A. Rounds, J.F. Pankow, Application of a radial diffusion-model to describe gas particle sorption kinetics, Environ. Sci. Technol. 24 (9) (1990) 1378–1386.
[15] C. Liu, S.S. Shi, C.J. Weschler, B. Zhao, Y.P. Zhang, Analysis of the dynamic interaction between SVOCs and airborne particles, Aerosol Sci. Technol. 47 (2) (2013) 125–136.
[16] Z. Guo, A framework for modelling non-steady-state concentrations of semivolatile organic compounds indoors - II. Interactions with particulate matter, Indoor Built Environ. 23 (2013) 26–43.
[17] Y. Xu, E.A.C. Hubal, P.A. Clausen, J.C. Little, Predicting residential exposure to phthalate plasticizer emitted from vinyl flooring: a mechanistic analysis, Environ. Sci. Technol. 43 (7) (2009) 2374–2380.
[18] S.R. McDow, Q.R. Sun, M. Vartiainen, Y.S. Hong, Y.L. Yao, T. Fister, Effect of composition and state of organic components on polycyclic aromatic hydrocarbon decay in atmospheric aerosols, Environ. Sci. Technol. 28 (12) (1994) 2147–2153.
[19] T. Ancelet, P.K. Davy, W.J. Trompetter, A. Markwitz, D.C. Weatherburn, Carbonaceous aerosols in an urban tunnel, Atmos. Environ. 45 (2011) 4463–4469.
[20] G.S. Casuccio, S.F. Schlaegle, T.L. Lersch, G.P. Huffman, Y. Chen, N. Shah, Measurement of fine particulate matter using electron microscopy techniques, Fuel Process. Technol. 85 (6) (2004) 763–779.
[21] M. Hussain, E. Tian, T.F. Cao, W.Q. Tao, Pore-scale modeling of effective diffusion coefficient of building materials, Int. J. Heat. Mass Transf. 90 (2015) 1266–1274.
[22] M. Wang, J. Wang, N. Pan, S. Chen, Mesoscopic predictions of the effective thermal conductivity for microscale random porous media, Phys. Rev. E Stat. Nonlin. Soft Matter Phys. 75 (3) (2007) 036702.
[23] A.A. Mohamad, Latice Boltzmann Method: Fundamentals and Engineering Applications with Computer Code, Springer Science & Business Media, 2011.
[24] Y.L. He, Y. Wang, Q. Li, Lattice Boltzmann Method: Theory and Application, Science, 2009. Beijing.
[25] J.Y. Xiong, Y.P. Zhang, X.K. Wang, D. Chang, Macro–meso two-scale model for predicting the VOC diffusion coefficients and emission characteristics of porous building materials, Atmos. Environ. 42 (21) (2008) 5278–5290.
[26] Y.T. Mu, L. Chen, Y.L. He, W.Q. Tao, Coupling finite volume and lattice Boltzmann methods for pore scale investigation on volatile organic compounds emission process, Build. Environ. 92 (2015) 236–245.
[27] L. Chen, G. Wu, E.F. Holby, P. Zelenay, W.Q. Tao, Q.J. Kang, Lattice Boltzmann pore-scale investigation of coupled physical-electrochemical processes in C/Pt and non-precious metal cathode catalyst layers in proton exchange membrane fuel cells, Electrochimica Acta 158 (2015) 175–186.
[28] K.J. Lange, P.C. Sui, N. Djilali, Pore scale simulation of transport and electrochemical reactions in reconstructed PEMFC catalyst layers, J. Electrochem. Soc. 157 (10) (2010) B1434–B1442.
[29] J. Yuan, B. Sundén, On mechanisms and models of multi-component gas diffusion in porous structures of fuel cell electrodes, Int. J. Heat. Mass Transf. 69 (2014) 358–374.